Evaluation of SmCo and SmCoN magnetron sputtering coatings for SOFC interconnect applications

Junwei Wu [a], Chengming Li [a,b], Christopher Johnson [c], Xingbo Liu [a,*]

[a] *Mechanical and Aerospace Engineering Department, West Virginia University, Morgantown, WV 26506, USA*
[b] *School of Material Science and Engineering, University of Science and Technology Beijing, Beijing 100083, China*
[c] *National Energy Technology Laboratory, Department of Energy, Morgantown, WV 26507, USA*

Abstract

Cobalt or cobalt containing coatings are promising for SOFC interconnect applications because of their high conductivity. We have investigated SmCo and SmCoN coatings deposited by magnetron sputtering from a SmCo (5% Sm) target on to Crofer 22 APU substrates. The composition, structure, surface morphology, and electrical conductivity of the coated substrates were characterized by SEM/EDX, XRD and ASR measurements. Addition of Sm enhances the oxidation resistance and the Cr retention capability of the coatings. The use of nitride as a precursor stabilizes Sm during oxidation of the films, thus inhibiting diffusion of Fe, resulting in a more compact coating and lowering ASR. The combined advantages of Sm addition to cobalt and the use of a nitride as a precursor, makes SmCoN coatings a promising new interconnect coating material.
© 2007 Elsevier B.V. All rights reserved.

Keywords: SOFC; Interconnect; Magnetron; Sputtering; SmCo; SmCoN

1. Introduction

Solid oxide fuel cell (SOFC) technology has become increasingly attractive as a power generation method because SOFC have lower emissions and higher efficiency relative to traditional energy-conversion systems. Interconnects are critical part of planar SOFC designs. The interconnect is needed to connect the individual cells in an SOFC stack electrically, and also separates air or oxygen on the cathode side from fuel on the anode side. Therefore, the requirements of interconnects are quite demanding, i.e., maintenance of high electrical conductivity, good stability in both reducing and oxidizing atmospheres, and close CTE match with other SOFC ceramic component [1–3].

Doped lanthanum chromite has been widely used as SOFC interconnect when operating at high temperature (∼1000 °C). However, these chromite interconnects are relatively expensive (especially for planar type stacks) as well as being brittle and difficult to fabricate [1,4]. The reduction in the operating temperature of SOFC from 1000 °C to 600–800 °C leads to the potential for using lower cost metallic interconnects materials such as stainless steel. Relative to their ceramic counterpart, metallic interconnects have improved stability, electrical conductivity, thermal conductivity, ease of manufacturing, and are less costly to manufacture [4]. Almost all of the candidate alloys being considered for this application are chromia forming alloys due to the acceptable electrical conductivity and stability of Cr_2O_3. However, as the scale for these alloys increases, scale electrical resistance also increases, and chromium evaporation can lead to cathode poisoning, and thus shorten the required service life for the SOFC stack. Newly developed alloys, such as [5] Crofer 22 APU (ThyssenKrupp VDM) and ZMG232 (Hitachi Metals), forming $(Mn,Cr)_3O_4$ spinel as the outer scale layer reduce this chromium volatility, but do not eliminate it entirely. These problems have prompted functional coatings development that can mitigate or eliminate these issues.

Vacuum deposition, especially physical vapor deposition, has been widely used to prepare protective coatings for SOFCs interconnect. Vacuum techniques have the advantage that they can easily deposit numerous types of coatings as well as the ability to control composition and morphology of a specific coating [6]. For interconnect applications, La–Cr–O coatings have been

---

* Corresponding author.
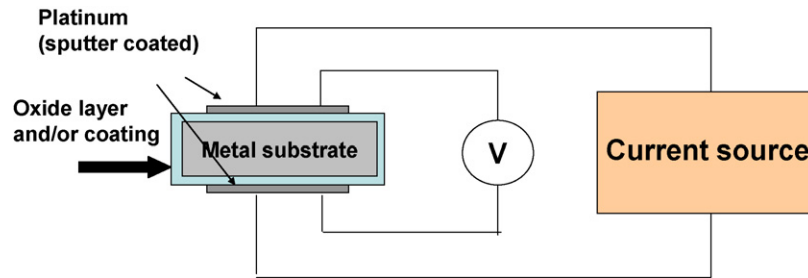 *E-mail address:* xingbo.liu@mail.wvu.edu (X. Liu).

Fig. 1. Schematic diagram of ASR measurement apparatus.

investigated using r.f. magnetron sputtering [7], laser assisted filtered arc deposition (LAFAD) has been used to deposit Cr–Al–N coatings [8] and multilayer Cr–Al–O–N coatings [9], and hybrid filtered arc-assisted electron beam physical vapor deposition (FA-EBPVD) has been used to deposit two-segment coatings of CrAlYO, and $(Mn,Co)_3O_4$ [10]. Preliminary measurements of ASR have shown acceptable values for these coatings, suggesting PVD methods are effective at producing high quality coatings for interconnect applications.

The use of rare earth element (RE) additives in bulk alloys or as surface treatments can improve creep resistance [11], and high temperature oxidation resistance [12] as well as refining alloy microstructure [13]. In SOFC interconnect fields, Ce/Co and Y/Co coatings deposited by a sol–gel method [14,15]; and Ce surface treatment by pack cementation [16,17] have been used to demonstrate the effectiveness of rare-earth surface modification on improving oxidation resistance, as well as lower power density degradation rates for "on-cell" tests.

In this work, Sm-doped coatings, SmCo and SmCoN, deposited by magnetron sputtering are studied using SEM/EDX, XRD and ASR measurements to characterize the coating before and after oxidation. The intent is to have Sm supply good oxidation resistance and Co to supply high conductivity [18,19] at SOFC operation temperature.

2. Experimental

2.1. Magnetron coating preparation

All film depositions were performed in dc mode using a high purity SmCo (5% Sm) target. Coatings were deposited on Crofer 22 APU coupons (acquired from ThyssenKrupp VDM) with the dimension of 1 cm × 2 cm × 1.5 mm. The surface was prepared by sanding with 1200grit SiC sand paper, followed by ultrasonic cleaning in acetone and alcohol prior to being placed on the rotating substrate holder. The distance between the targets and the substrates was kept constant at 30 mm. To enhance adhesion, all substrates were baked to 230 °C for 30 min. After a base pressure of 3E − 3 Pa was obtained, high purity Ar gas (99.999%) was let into the chamber until a pressure of 2 Pa was achieved.

For the SmCoN coating, in order to improve the adhesion between film and substrate, SmCo transition layers about 100 nm thick were deposited on the substrates prior to introduce reactive gas, N_2. The ratio of argon to nitrogen was kept as 1:4 during deposition. The total thickness of SmCo and SmCoN coatings were ∼2.5 μm. EDX analysis showed the ratio of (Sm/Sm + Co) for both the nitride and non-nitride coatings was around 12 at.% in the as-deposited state.

2.2. Coatings characterization

The area-specific resistance (ASR) measures the resistance metal substrate, as well as the electrical properties of the oxide layers. However, since the electrical resistance of the substrate is negligible relative to the oxide layers the measured values can be considered those of the oxide coatings. The ASR test is a 4-wire resistance measurement, as shown in Fig. 1. The tests were done using both constant current (40 mA) and temperature (700 °C or 800 °C) measurements for degradation evaluation, as well as multiple temperature measurements (600–900 °C at 50 °C intervals) for activation energy measurements. By measuring ASR as a function of temperature over this range, the activation energy for electronic conduction (E_a) can be obtained as below.

$$\frac{ASR}{T} = A\, e^{E_a/2kT} \tag{1}$$

Therefore,

$$Log\left(\frac{ASR}{T}\right) = \frac{E_a}{2kT} + Log\, A \tag{2}$$

where the slope of Log (ASR/T) versus 1/T is equal to $E_a/2k$, with k being Boltzmans constant with units of J/K and 1 J = 6.241E18 eV.

Annealing of the coated substrates was done in air for 100 h at 700 and 800 °C. After annealing, the samples were analyzed with SEM/EDX, and XRD, and the results with the as-deposited coatings. Finally, samples were mounted in epoxy, sectioned, and polished for analysis of the cross-sections by SEM/EDX.

3. Results and discussion

3.1. X-ray diffraction

The XRD analysis of SmCo and SmCoN films in the as-deposited state and after oxidation are shown in Fig. 2. The as-deposited coatings both display a typical amorphous pattern in the XRD (not shown here). After oxidation at 700 and 800 °C, the diffraction patterned indicates the formation of Co_3O_4, $CoFe_2O_4$ and $SmCoO_3$ in both samples. Based on previous experience, it
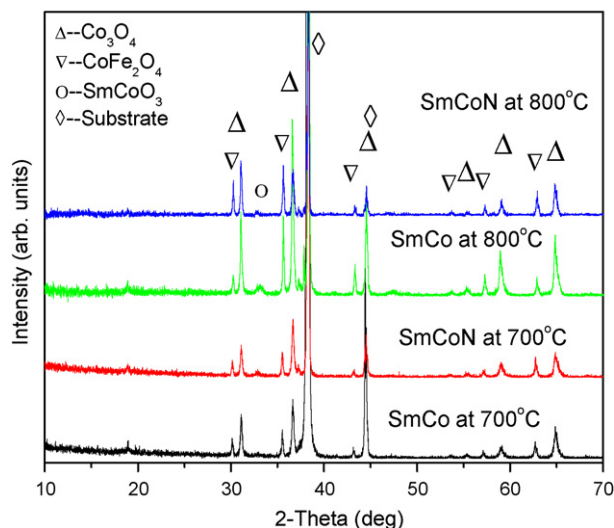
Fig. 2. XRD patterns of SmCo and SmCoN as-deposited and after oxidation.

was also expected that small amounts of $(Mn,Cr)_3O_4$ and Cr_2O_3 would be present, however, these phases would be present at the interface between the coating and substrate, and thus the diffraction from these layers would be attenuated by the coating material. Thus while $(Mn,Cr)_3O_4$ and Cr_2O_3 may be present, as indicated by the weak peak at 33° two-theta, we have labeled this as $SmCoO_3$ in Fig. 2 because of the surface proximity of Sm and Co.

3.2. Surface morphology

Surface morphology of SmCo and SmCoN as-deposited coatings are shown in Fig. 3(a) and (b). These images show that the films as-deposited are quite uniform and that the particles are less than 100 nm in size. There are also some cracks in the coatings, which may be due to stresses developed during the coating process.

After oxidation at 700 °C for 100 h (Fig. 3(c) and (d)), the films become flatter and more uniformly structured with no cracks present. The SmCo film forms particles with a uniform size of around 0.5 μm, and the SmCoN coating shows a relatively smooth surface with no obvious appearance of particle size increase. For oxidation at 800 °C (Fig. 3(e) and (f)), the microstructure of SmCo coating shows a mixture of some fine grained structures and some cubic particle clusters. While for the SmCoN coating, the surface still shows a small uniform grain size. Generally, both coatings after oxidation are quite dense and compact, and SmCoN coating appears somewhat finer grained than the SmCo coating.

EDAX analysis of the surfaces after oxidation at 700 and 800 °C, indicates that the surface contains primarily Fe and Co with small amounts of Sm, Cr, Mn. The surface concentrations of latter three elements are very low in both the SmCo film and SmCoN films (less than 1% is measured by EDX). The Fe/Co ratio (at.%) at the surface was significantly different for the different annealing temperatures, both films showed around 15% Fe at the surface at 700 °C, and this increase to around 30%

at 800 °C. Moreover, the Fe concentration is even higher for the clusters of cubic structures found on the SmCo coating annealed at 800 °C (around 50%), suggesting that at higher temperature Fe diffuses more readily, and thus it can then be expected that more $CoFe_2O_4$ spinel is formed at the surface.

3.3. Cross-section and elemental distribution along scale/substrate interface

The cross-section view for both coatings shows them to be continuous and without voids [20], as shown in Fig. 4. The linescan results indicated that after oxidation at 700 °C (Fig. 4a) and 800 °C (Fig. 4b) the coatings exhibited an outermost Fe-rich layer, with the exception of the SmCoN coating oxidized at 700 °C, which shows a uniform composition distribution. This is similar to previous work on the CrAlON coating system [9], in which the nitride precursors were effective Fe diffusion barriers. The X-ray counts outer surface shows a higher Co/Fe ratio than would be expected for a stoichiometric $CoFe_2O_4$ spinel phase suggesting the outermost layer may be a mixture of $CoFe_2O_4$ and Co_3O_4. Below the outer layer the coatings is mainly composed of Co, O, overlapped with a continuous period of low level Sm, which would be expected to be Co_3O_4 and $SmCoO_3$, as was indicated by the XRD results. At the interface between the substrate and coating there is a small peak of Mn and a slight enrichment of Cr, consistent with $MnCr_2O_4$ formation, although this is not apparent in the XRD data. Except for the Cr found at the interface, there is no chromium throughout the coating layer, even after 100 h at the test temperature, suggesting that the coatings are an effective diffusion barrier to chromium diffusion (Table 1).

3.4. Electrical resistance

ASR measurements reflect both the conductivity and the thickness of surface layer (oxide scale and/or coatings); it is generally assumed that the resistivity of the substrate alloy is negligible compared with that of the coatings on the surface. In addition, the current applied (40 mA) is relatively small, making interfacial polarization and local heating negligible. Therefore the measured ASR is assumed to be due only to oxide coating.

Fig. 5 displays ASR versus time for comparison of SmCo and SmCoN coating at 700 and 800 °C. At the beginning, the ASR drops significantly, probably due to densification of the platinum during the initial test period. After the minimum is reached, the ASR slowly increases, and follows an approximately parabolic behavior. Note that the SmCoN has a significantly lower ASR than the simple SmCo coating at both 700 and 800 °C. At both temperatures, the SmCo coating is still increasing significantly after 100 h, while the SmCoN coating begins to approach a constant value in the sample heated at 800 °C. Note there is a discontinuity present on SmCoN ASR curves at 800 °C around 40 h (Fig. 5(b)). The reason for this event is not clear, but may be due to improved contact between the mesh, paste or samples.

After the test, the apparent activation energy was calculated based on Eq. (2) for both coatings and the results are shown in Fig. 6. Both coatings are very close in apparent activation
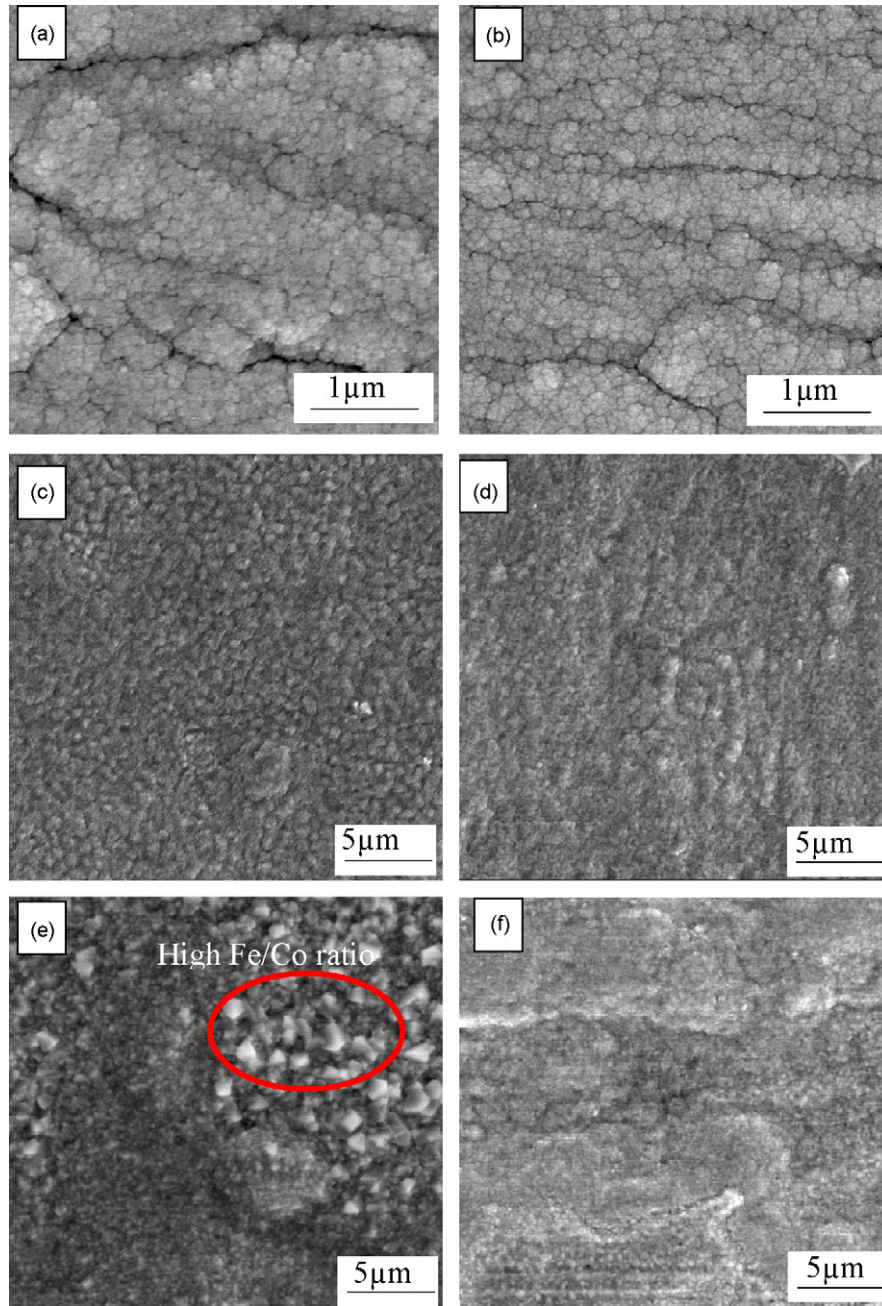
Fig. 3. SEM images of SmCo and SmCoN coatings (a, c, e are SmCo coating; b, d, f are SmCoN coatings) (a, b) as-deposited (c, d) oxidized at 700 °C for 100 h (e, f) oxidized at 800 °C for 100 h.

energy at 700 °C. At 800 °C, the apparent activation energy of SmCo is considerably higher than that of SmCoN, which may account in some part for the trend in the ASR values, SmCo (800 °C) > SmCoN (800 °C) > SmCo and SmCoN (700 °C).

Table 1
Whole coating and top Fe-rich zone thickness after oxidation (unit: μm)

	As-deposited	700 °C		800 °C	
		Whole	Fe-rich zone	Whole	Fe-rich zone
SmCo	3.0	4.5	1.5	4.2	1.5
SmCoN	3.0	4.0	0	4.0	0.5

4. Discussion

4.1. Influence of temperature on coating oxidation

Based on the data previously discussed, the structures of both coatings after oxidation can be schematically displayed as in Fig. 7. The SmCo coating evaluated at 700 and 800 °C and the SmCoN coating tested at 800 °C, corresponds to Fig. 7(a). Three distinct layers are present, a top layer of CoFe$_2$O$_4$ and Co$_3$O$_4$, a main layer of Co$_3$O$_4$ and SmCoO$_3$, and a thermally grown sub-layer of MnCr$_2$O$_4$ and Cr$_2$O$_3$. For the SmCoN coating tested at 700 °C only the main layer and the sub-layers are
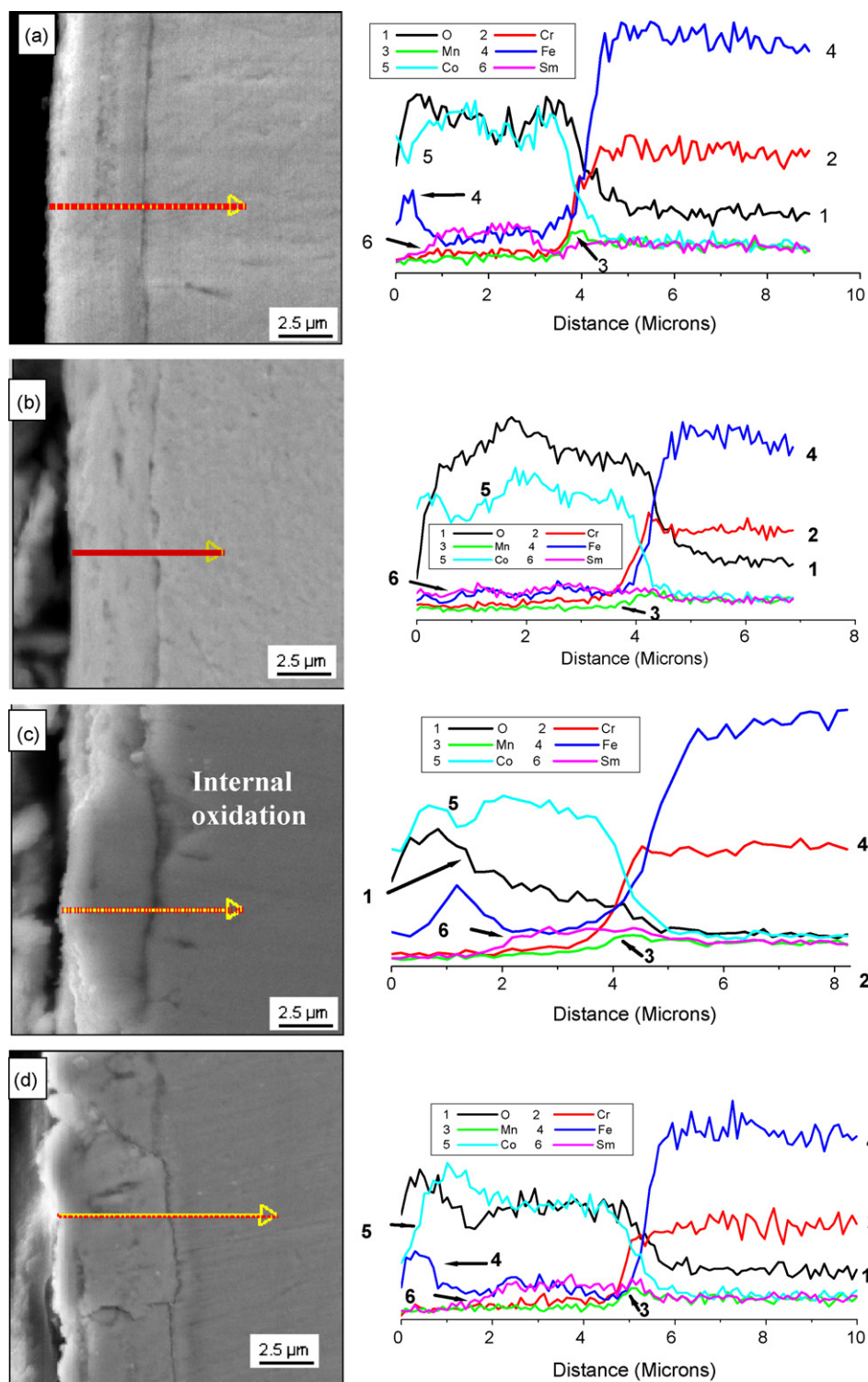
Fig. 4. Secondary electrons cross-sections images and linescan of coatings after oxidation (a) SmCo coating after oxidation at 700 °C for 100 h; (b) SmCoN coating oxidized at 700 °C for 100 h; (c) SmCo coating after oxidation at 800 °C for 100 h; (d) SmCoN coating oxidized at 800 °C for 100 h.

present, no outer $CoFe_2O_4$ is present. These structures suggest that there is only inward oxygen diffusion and outward Fe diffusion in the three samples corresponding to Fig. 7(a). The inner diffusion of oxygen plays a more important role in the oxidation process, and may be used to explain trends in the ASR behavior. For instance, Co_3O_4 which is a major phase in all

samples, has a relatively high conductivity of 35.5 S cm^{-1} at 800 °C, while $CoFe_2O_4$ has low conductivity of 0.35 S cm^{-1}, however, since the outer layer is mixed, it would not affect the overall conductivity since Co_3O_4 can act as the conducting pathway in the outer layer. However, thermally grown oxide layers below the main layer will be continuous layers and
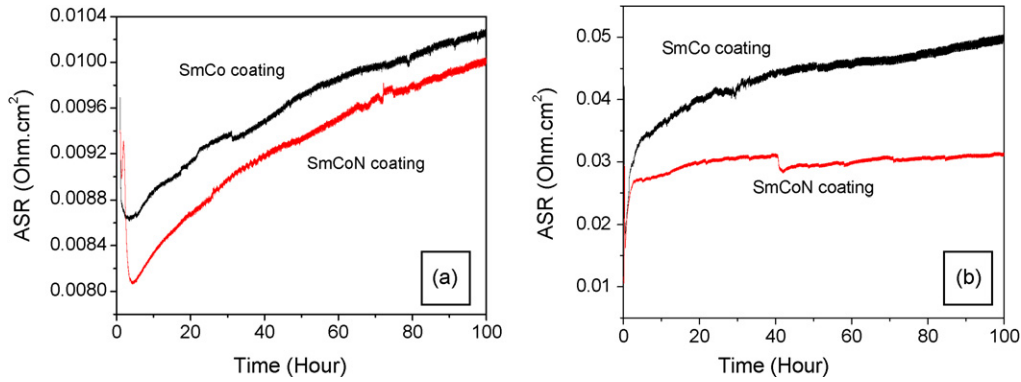
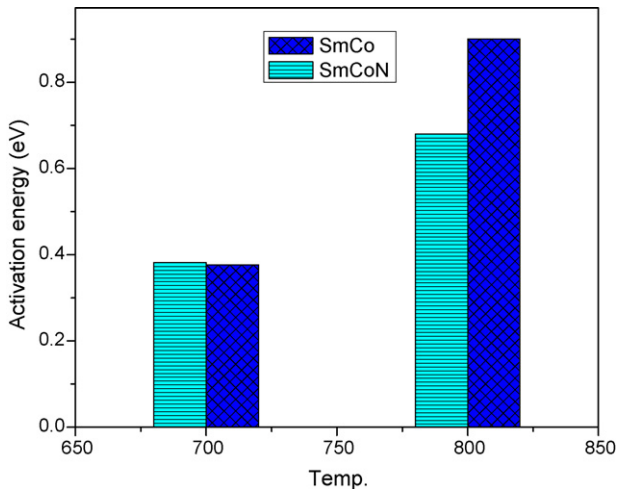Fig. 5. ASR of SmCo and SmCoN coating for 100 h: (a) 700 °C and (b) 800 °C.

Fig. 6. Activation energy of SmCo and SmCoN coating after oxidation at 700 °C and 800 °C for 100 h.

are lower in conductivity, such as $MnCr_2O_4$ (0.05 S cm^{-1} at 800 °C), Mn_2CrO_4 (12.8–30.3 S cm^{-1} at 750 °C) and Cr_2O_3 (0.13 S cm^{-1} at 800 °C) [19]. Thus it is expected that the growth of the less conductive phases at the substrate/coating interface will determine to a large extent the final ASR values. At 700 °C, both ASR curves obey the approximate parabolic law, which describes diffusion control of oxidation process, and thus the increase in ASR is likely due to the continuing growth

of $MnCr_2O_4$ or Cr_2O_3. While at 800 °C, the ASR difference between SmCo and SmCoN becomes larger, both curves are rather flat, which reflects a stable or semi-stable oxidation phase having been reached. The higher temperature has resulted in a stable thermally grown sub-layer being reached sooner, and thus the ASR curve is relatively flat.

4.2. Effect of Sm on coating

The rare earth metals (RE), including Sm, as material additives primarily improve the creep resistance, corrosion resistance and high temperature oxidation resistance of materials. Sm has also been used in SOFC applications as a dopant for ceria-based electrolytes, and a component in perovskite cathode materials. Doping ceria with Samaria (Sm_2O_3) induces the least distortion of the parent lattice due to having the optimum radius, which causes no expansion or contraction in the ceria lattice [21]. As a component in an interconnect coating, it is supposed that Sm increases conductivity and provides higher oxidation resistance for metallic interconnects. It may be more compatible from a stability standpoint with some of the more advanced electrolytes and cathode materials mentioned above.

Results of pure cobalt coatings obtained by means of dip coating [14,15] and electroplating [22], show linear increase of ASR values during the initial 100 h at 750 and 800 °C, respectively, indicating the pure cobalt films have low oxidation resistance at high temperature. Ultimately the substrate material will grow a
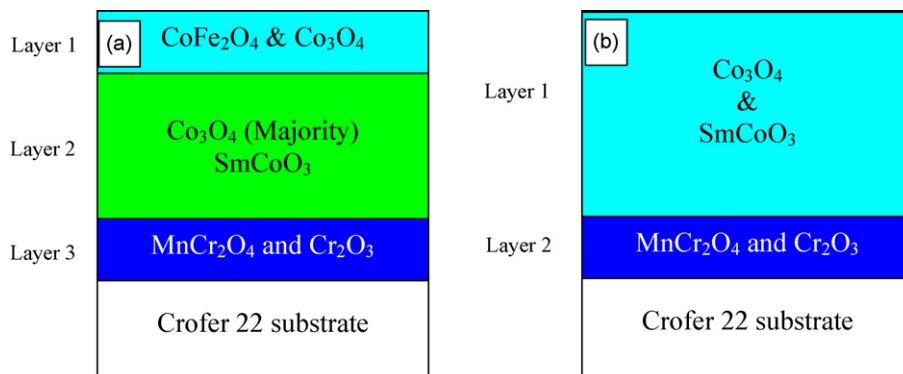

Fig. 7. Schematic structure of oxidation layers after 100 h oxidation. (a) Applicable to SmCo (700 and 800 °C), SmCoN (800 °C) and (b) applicable to SmCoN (700 °C).

thick enough thermal sub-layer to provide a stable oxide, however these layers typically are phases with low conductivity. Thus having coatings with good conductivity and with improved oxidation resistance is beneficial to overall performance. Comparison of the pure Co_3O_4 film result with SmCoN and SmCo in Fig. 5, at 800 °C one can see that ASR of both coatings almost remain unchanged or change little after just 50 h. Therefore, it can be concluded that cobalt coatings doped with Sm provides improve oxidation resistance.

Chromium evaporation is also an important issue in SOFC. Co_3O_4 has proven a good coating for reducing the evaporation of chromia, Cr retention is improved more than 90% compared to pure Cr_2O_3 after oxidation of 500 h at 800 °C [19]. However at high temperature, Co_3O_4 will be replaced completely at the coating surface by $(Co,Cr)_3O_4$ even after 220 h for 100 μm thick Co coating [22] due to chromium diffusion. Although chromium retention was enhanced and $(Co,Cr)_3O_4$ is a relatively stable phase, there is still risk of chromium evaporation. For the SmCo and SmCoN coatings, it is obvious from the linescan data that there is no Cr in the coating layers, which suggests Co-doped with Sm reduces the chromium evaporation significantly.

4.3. Advantage of nitride coating

For Cobalt nitride vacuum deposition, different P_{N_2}/P_{Ar} can produce different nitride coatings, such as Co_4N, Co_3N, Co_2N, Co_3N_2 or CoN, and all of these compounds have good conductivity at room temperature [23,24]. Introduction of Sm into the Co–N coating will change the stoichiometry significantly. As a nitride forming element, Sm thermodynamically favors an arrangement where the nitrogen atoms occupy the sites surrounded by as much Sm atoms as possible [25]. At high temperature, decomposition will occur first before oxidation in ambient environment, SmCoN directly decomposes into Sm nitride and solid solutions of Co and nitrogen according to reaction (3), immediately followed by reaction (4), which results in degasifying of solid solution to form pure cobalt.

$$(SmCo)N \rightarrow SmN_y + (Co-N_x) \tag{3}$$

$$(Co-N_x) \rightarrow Co + (x/2)N_2\uparrow \tag{4}$$
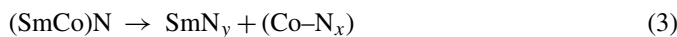
SmN will remain stable until around 700 °C [26], explaining why no Sm depletion zone was found at 700 °C of SmCoN. At higher temperature (800 °C), SmN begins to decompose according to reaction (5).

$$SmN_y \rightarrow Sm + (y/2)N_2\uparrow \tag{5}$$

At this high temperature, Sm not only begins to evaporate, but can be oxidized readily, and the decomposition of the nitride controls the rate at which it is released. In the SmCo coating at the same temperature, the Sm has enough time to evaporate before oxidation, which results in an increased depletion of Sm at the surface of the sample. At the same time, from the linescan results, a Fe-rich outer layer is overlapped with Sm depletion zone, however, both are thinner in the SmCoN coatings and no Fe diffusion was found of SmCoN at 700 °C. Thus, the benefits of using a SmCoN coatings as a precursor for SmCo oxide for-

mation rather than a simple SmCo alloy layer is that the nitride has improve Sm retention, and thus forms a more complete oxide layer, this in turn leads to improve oxidation resistance for the substrate and a lower ASR. The nitride coating also inhibits Fe migration, most likely due to the more compact and denser nature of nitride relative to the sputtered SmCo layer, as can be seen from both the top view and cross-section SEM images.

Therefore, the combined advantages of Sm addition to Co_3O_4 and the use of a nitride precursor in the form of SmCoN coatings is that it results a denser oxide coating, provides higher oxidation resistance, higher Cr retention capability, and low ASR, and thus is promising for real interconnects applications.

5. Conclusions

(1) Nanoparticles of SmCo and SmCoN coatings were fabricated successfully by magnetron sputtering. SmCo particle size increases with increase of oxidation temperature, while no obvious particle size increase was observed for SmCoN coatings. For both coatings, no spallation and cracks were observed.

(2) XRD and cross-section linescan show three layers for SmCo (700 and 800 °C), SmCoN (800 °C) after 100 h oxidation, with a the top layer made of $CoFe_2O_4$ and Co_3O_4, Co_3O_4 and $SmCoO_3$ in middle layer, and thermally grown $MnCr_2O_4$ (and possibly Cr_2O_3) formed at the substrate coating interface. For the SmCoN coating oxidized at 700 °C, only two layers are present, a Co_3O_4 and $SmCoO_3$ top layer, and $MnCr_2O_4$ as the sub-layer. No $(Co,Cr)_3O_4$ was found in any of the layers, demonstrating the chromium blocking ability of the coatings.

(3) ASR of SmCo and SmCoN coatings at 800 °C show little or no change after 50 h oxidation, suggesting that a stable oxidation state has been reached.

(4) At both 700 and 800 °C, ASR of oxide formed from SmCoN is lower than that of simple SmCo coatings, because introduction of N_2 forms SmN during deposition, which remains stable even at 700 °C, therefore compared to SmCo coatings, the SmCoN coatings have a controlled oxidation process as the nitride decomposes leading to more compact and denser coatings, thinner Sm depletion zones, less Fe diffusion into outmost layer, and higher conductivity.

References

[1] W.Z. Zhu, S.C. Deevi, Mater. Sci. Eng. A (2003) 227–243.
[2] Z. Yang, G.-G. Xia, G.D. Maupin, et al., Surf. Coat. Technol. 201 (2006) 4476–4483.

[3] Z. Yang, K. Scott Weil, D.M. Paxton, J.W. Stevenson, J. Electrochem. Soc. 150 (2003) A1188–A1201.

[4] W. Vielstich, A. Hubert, M. Gasteiger, A. Lamm, Handbook of Fuel Cells—Fundamentals, Technology and Applications: Fuel Cell Technology and Applications, Wiley, New York, 2003 (Chapter 74).

[5] Z. Lu, J. Zhu, E. Andrew Payzant, M.P. Paranthaman, J. Am. Ceram. Soc. 88 (4) (2005) 1050–1053.

[6] L.R. Pederson, P. Singh, X.D. Zhou, Vacuum 80 (2006) 1066–1083.

[7] N. Orlovskaya, A. Coratolo, C. Johnson, R. Gemmen, J. Am. Ceram. Soc. 87 (2004) 1981–1987.

[8] P.E. Gannon, C.T. Tripp, A.K. Knospe, et al., Surf. Coat. Technol. 188–189 (2004) 55–61.

[9] A. Kayani, R.J. Smith, S. Teintze, et al., Surf. Coat. Technol. 201 (2006) 1685–1694.

[10] P.E. Gannon, V.I. Gorokhovsky, M.C. Deibert, Int. J. Hydrogen Energy 32 (2007) 3672–3681.

[11] D. Wenwen, S. Yangshan, M. Xuegang, X. Feng, Z. Min, W. Dengyun, Mater. Sci. Eng. A 356 (2003) 1–7.

[12] R. Thanneeru, S. Patil, S. Deshpande, S. Seal, Acta Mater. 55 (2007) 3457–3466.

[13] M.A. Dudek, R.S. Sidhu, N. Chawla, M. Renavikar, J. Electron. Mater. 35 (2006) 2088.

[14] W. Qu, J. Li, D.G. Ivey, J. Power Sources 138 (2004) 162–173.

[15] W. Qu, L. Jian, D.G. Ivey, J.M. Hill, J. Power Sources 157 (2006) 335–350.

[16] D.E. Alman, P.D. Jablonski, Int. J. Hydrogen Energy 32 (2007) 3743–3753.

[17] D.E. Alman, C.D. Johnson, W.K. Collins, P.D. Jablonski, J. Power Sources 168 (2007) 351–355.

[18] X. Chen, P.Y. Hou, C.P. Jacobson, et al., Solid State Ionics 176 (2005) 425–433.

[19] M. Stanislowski, J. Froitzheim, L. Niewolak, et al., J. Power Sources 164 (2007) 578–589.

[20] G. Cabouro, G. Caboche, S. Chevalier, P. Piccardo, J. Power Sources 156 (2006) 39–44.

[21] S. Phok, R.N. Bhattacharya, Phys. Status Solidi A 203 (15) (2006) 3734–3742.

[22] X. Deng, P. Wei, M. Reza Bateni, A. Petric, J. Power Sources 160 (2006) 1225–1229.

[23] J.-S. Fang, L.-C. Yang, C.-S. Hsu, et al., J. Vac. Sci. Technol. 22 (2004) 698–704.

[24] W. De La Cruz, O. Contreras, G. Soto, E. Perez-Tijerina, Revista Mexicana De Fĩlsica 52 (2006) 409–412.

[25] S. Stoyanov, V. Skumryev, Y. Zhang, et al., J. Appl. Phys. 93 (2003) 7592–7594.

[26] F.A. Cabral, S. Gama, E. de Morais, et al., IEEE Trans. Magn. 32 (1996) 4365–4367.